Membrane integrated valorization of waste dairy whey: A novel technique

Pallabi Das (pallabidasemail3@gmail.com)
CIMFR: Central Institute of Mining and Fuel Research CSIR
Suman Dutta
IIT (ISM): Indian Institute of Technology
Sudip Maity
CIMFR: Central Institute of Mining and Fuel Research CSIR

Research Article

Keywords: Waste Valorization, Lactose Recovery, Cheese Whey, Membrane Crystallization (MCr), Process Intensification, Sustainable Technology

Posted Date: July 25th, 2022

DOI: https://doi.org/10.21203/rs.3.rs-1850229/v1

Membrane integrated valorization of waste dairy whey : A novel technique

P. Das[1]*, S. Dutta[2], S. Maity[1]

1: CSIR-Central Institute of Mining and Fuel Research, Barwa road campus, Dhanbad-826015, Jharkhand, India

2: IIT-Indian School of Mines, Police Line, Sardar Patel Nagar, Hirapur, Dhanbad, Jharkhand 826004, India

Corresponding author email: pallabidasemail3@gmail.com

Corresponding author institutional address: CSIR-Central Institute of Mining and Fuel Research, Barwa road campus, Dhanbad-826015, Jharkhand, India

Graphical Abstract

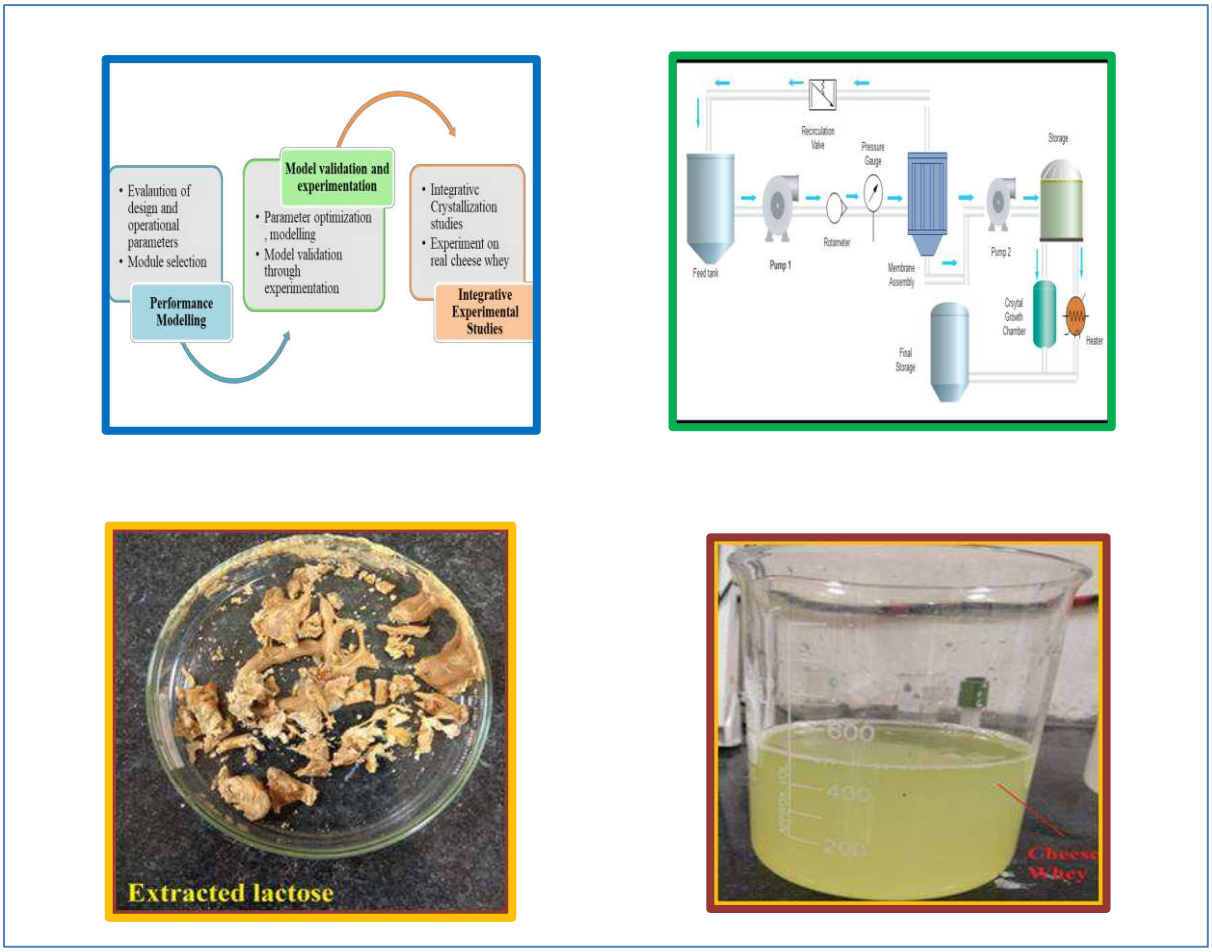

Abstract

Experiments were undertaken to develop a sustainable, process intensified membrane integrated crystallization technique for the extraction of lactose from cheese whey. The study explored concentrative mode of membrane crystallization and its possible integration with conventional evaporative crystallization. Effects of the membrane module, mass transfer coefficient, nucleation rate, pressure drop and their interdependence were studied through modelling and system design. This was followed by exhaustive experimental investigations and parameter optimization. The effect of antisolvent addition on membrane crystallization was also explored. Following this, the membrane integrated technique was employed for selective lactose recovery from real cheese whey sourced from sweetmeat manufacturers. Competitive lactose crystal yields of 3.8- 4.96 g per 100 ml of cheese whey (from which fat &

protein content was isolated) were obtained. The presence of membrane lowered the total crystallization times as compared to evaporative crystallization. Addition of antisolvent reduced crystallization times in the range of 13.5% - 23.1% for membrane integrated & chemical precipitation techniques. In the alcohol series of antisolvent dosing , a progression from methanol to butanol demonstrated enhanced reduction in crystallization. Crossflow NanoFiltration (NF) showed a higher concentration than crossflow UltraFiltration (UF). The membrane integrated crystallization technique successfully demonstrated waste valorization with competitive lactose yields from cheese whey.

Keywords: Waste Valorization, Lactose Recovery, Cheese Whey, Membrane Crystallization (MCr), Process Intensification, Sustainable Technology

1. Introduction

Crystallization is a ubiquitous process in the chemical industry that finds applications in almost all major chemical production processes ranging from sugar production, fertilizer synthesis, and pharmaceuticals to soap production. It is an essential unit operation for purification, separation, and manufacture of the final product. Crystallization can be achieved by evaporation, freezing, application of vacuum, etc. The most common crystallization approach in the industry involves evaporative crystallization wherein a series of forward/backward or mixed feed evaporators perform stage-wise solvent evaporation. Design variants include i) forced circulation crystallizers with separate boiling and external heating zones for the slurry, ii) Draft tube baffle crystallizer where mixing /stirring operations are induced by propeller for better contact of circulated slurry and the liquid. There are several drawbacks faced by these systems; the principal being high energy consumption and low process efficiency [1, 2]. Often, precise control of crystal size and distribution becomes a problem in large scale industrial

crystallizers. Furthermore, these large scale systems are tailor-made for a narrow range of process conditions, making it difficult to operate under fluctuating load variations.

It is precisely this gap that MCr systems address. Firstly, the fundamental drawback of high energy consumption and low efficiency is ameliorated. Secondly, membranes provide a high contact surface for mass transfer. The compact process design enables a multipass contacting single system. Thirdly, the membrane surface aids in heterogeneous nucleation lowering the energy barrier needed to reach the spontaneous nucleation stage. This cuts the overall energy requirement for the entire process. Finally, membrane-based systems allow more precise control over the crystal size distribution since the rate of nucleation can be controlled [3, 4]. Interestingly, a host of different MCr systems like pressure-induced dewatering, osmotic concentration difference, induced preferential solvent removal, salting out of target species by antisolvent addition; does not include any kind of external heat addition. This makes it possible to avoid the degradation of the heat-sensitive elements present in the crystal matrix [5, 6].

In terms of practical implementation and process development, membrane systems offer high operational flexibility allowing easy coupling and decoupling of membrane modules as per the process needs. Multiple unit operations can be merged, leading to the emergence of smaller, cleaner, and more efficient options [7, 8]. Such modular units characterized by a high degree of process intensification can be integrated with the existing technology options. This forgoes the prerequisite of scraping existing infrastructure for integrative applications. These process intensified options can be used in conjunction with conventionally prevalent systems.

MCr can operate in two different modes: i) nucleation and allied growth of the crystal in the membrane surface and ii) dewatering based concentration to reach nucleation and ultimate crystal growth. The latter offers the choice of concentration up to saturation and/or supersaturation and the possibility of integration with conventional unit operations.

Furthermore, the latter offers relatively higher operational flexibility for membrane cleaning, module addition, and fabrication of system infrastructure. Therefore, it was selected as the core of the process design which was modelled and experimented upon. While designing Membrane Crystallization (MCr) processes, optimization of process parameters and their synchronization with key crystallization parameters like nucleation rate, mass transfer coefficient is of prime importance. To understand the process dynamics, it is imperative to undertake detailed performance modelling. Based on the modelling trends, the experimental design is formulated.

One of the important applications of MCr is in the domain of value-added product recovery. MCr techniques have been employed for the recovery of brine, vitamins, selective concentration of pharmaceuticals fruits and other heat-sensitive feedstocks [9, 10,11]. The application of membranes operating at ambient temperatures and pressures prevents any denaturation of sensitive feedstocks. Besides ensuring sustainable process operation, resource recovery through MCr promotes waste valorization. Waste valorization in different domains is an extremely burning research topic as it leads to simultaneous waste management and resource conservation [12, 13]. The application of MCr in the domain of waste valorization has the potential to cause a paradigm shift in the research area due to the eco-friendliness and high efficiency. Experiments targeting resource recovery from different wastewater streams that are widely available and contain a considerable amount of valuables needs to be taken up urgently.

One such nutrient-rich wastewater stream that is often wasted is cheese whey. Cheese whey emanates from cheese manufacturing units and sweetmeat productions. Cheese whey contains nutrients, proteins, fats and lactose [14]. Lactose is one of the principal components with lactose % ranging from 8-10% [15]. This lactose constituent is a valued resource possessing multifarious applications, especially in the feed industry. This makes research efforts towards lactose extraction from cheese whey all are more imperative.There have been previous efforts for lactose recovery from cheese whey utilizing fermentation pathways, chemical precipitation

and ion exchange/ filtration techniques [16,17, 18]. Researchers have also tried to treat dairy wastewater and recover valuables like succinic acid from cheese whey [19, 20, 21]. However, the potential of MCr towards lactose extraction from cheese whey remains relatively unexplored.

Here, in this study, we focus on the development of a process intensified, sustainable membrane integrated technique for extraction of the lactose from cheese whey. Prior to experimentation, exhaustive modelling was undertaken to develop a membrane integrated crystallization approach that can be coupled with conventional evaporative crystallization. Simultaneously process dynamics of concentrative MCr was also evaluated. The modelling trends were validated with experimental investigations and parameter optimizations to develop the membrane integrated technique. Finally, it was applied towards lactose extraction from real cheese whey sourced from sweetmeat manufactures. The addition of antisolvent on the process of lactose recovery and the role of nature and quantity of antisolvent on crystallization time and yields were also explored.

2. Modelling Study:

2.1 Approach

i) To make the model as representative of a real-life system as possible, real-time data from the membranes and other process data were incorporated.

ii) Modification of equations like ENP (Extended Nerst Planck Equation), Pore flow model was undertaken to suit the specific features of the system.

iii) Concentration polarization modulus was integrated to describe the real-time operational problems encountered in membrane systems.

iv) The relationship of pressure drop, rate of nucleation on the system performance were studied.

v) Different configurations were studied to undertake a comparative performance evaluation.

vi)The effect of both internal properties, as well as external factors, was assimilated.

vii) An iterative procedure with error analysis and updating of values were created, till minimum error was attained

2.2 Model development

The modelling and design optimization was undertaken stage-wise to represent a real-life system as closely as possible.

At first sizing estimation for process design was undertaken such as optimization of the number of fibres in the Hollow Fibre (HF) bundle, feed spacer width, channel depth, and permeate spacer placements. The effect of these on flux was evaluated. The same method was followed for both HF and spiral-wound modules.

Following this different process variables like flow rate, Transmembrane Pressure (TMP), feed concentration and volume were optimized. For transport of mass and hydrodynamics, the Extended Nerst Planck equation was used. This enabled flux calculation combining mass and hydrodynamic factors. Real-life performance indices like concentration polarization modulus, the effect of pressure drop were included. The effect of these factors on the solvent flux was assessed.

Simultaneously interdependence of the parameters and their effect on flux was studied with the help of artificial neural network modelling. The effect of this input variable on flux was studied using an exponential function

The last module was a separate block for crystallization wherein the effect of parameter and process dynamics on crystallization transfer coefficient was evaluated. Also, crystal growth dynamics like nucleation rate supersaturation ratio was optimized for optimum performance

Finally, a performance modelling block was utilised to bridge between the optimized design and optimized operational parameters like channel velocity mass transfer coefficient and solute diffusion.

The results obtained from different modules were combined to build an integrated performance model for a MCr system

2.2.1. Parameter Optimization Module

Porosity distribution:

$$\varepsilon = \frac{\text{Volume of pores on 1 fibre}}{\text{total volume of membrane}} = \frac{n\pi\left(r_i\right)^2 L}{L\pi\left(\left(r_o\right)^2 - \left(r\right)^2\right)} \qquad \text{Eqn. 1}$$

Width of a feed spacer channel

$$\varepsilon = \frac{\text{Volume of pores on 1 fibre}}{\text{total volume of membrane}} = \frac{n\pi\left(r_i\right)^2 L}{L\pi\left(\left(r_o\right)^2 - \left(r\right)^2\right)} \qquad \text{Eqn. 2}$$

Cross- sectional areas

$$A_f = H_f * W \qquad \text{Eqn. 3}$$

$$A_p = H_p * L \qquad \text{Eqn. 4}$$

Estimation of flux using modified pore flow model. Variation of transmembrane pressure with distance was also incorporated [22]

$$J_v = k_1 \Delta P(x) + k_2 \Delta P(x)$$ Eqn.5

Where,

$$k_1 + k_2 = \frac{N n \varepsilon (r_i)^2}{8 \eta \delta}$$ Eqn. 6

2.2.2. Process Performance Module

Estimation of flux by Extended Nerst Planck Equation: [23]

$$J_i = -k_{c,i}(C_m - C_b) + J_v C_m$$ Eqn.7

Solute concentration at the vicinity of the membrane [24]

$$\frac{C_m - C_p}{C_b - C_p} = e^{\frac{Jv}{kS}}$$ Eqn. 8

Pressure variation with position [25]

$$A_f = H_f * W$$ Eqn.

9

Eqn4

,

$$\lambda = \frac{4}{\left(r^3 * R_m\right)^{0.5}}$$ Eqn. 10

Calculation of velocity:

$$V_f = \frac{F_i}{A}$$ Eqn. 11

Evaluation of mass transfer coefficient [26]:

$$S_h = 1.62\left(\frac{d_i * R_e * S_c}{L}\right)^{0.33}$$ Eqn. 12

where

Sherwood number

$$S_h = \frac{kd_i}{D}$$ Eqn. 13

Eqn 12

Reynolds Number:

$$R_e = \frac{\rho V_f d_i}{\eta}$$ Eqn. 14

Schmidt Number:

$$S_c = \frac{\eta}{\rho D} \qquad \text{Eqn. 15}$$

Estimation of structural parameter:

$$S = \frac{E\tau A}{\delta W} \qquad \text{Eqn. 16}$$

Calculation of solute flux by modified Extended Nerst Planck (ENP) equation [27]

$$\Phi_i = \frac{J_v}{kS} \qquad \text{Eqn. 17}$$

Calculation of pressure drop in the feed side: [28]

$$\Delta P_{f,L}(z) = \frac{f_D * Z * \rho * V_{f(z)^2}}{d_i * 2} \qquad \text{Eqn. 18}$$

$$f_D = \frac{64}{R_e} \qquad \text{Eqn. 19}$$

2.2.3 Crystallization Module

Nucleation rate was estimated from crystal density and growth rate. The growth rate was evaluated using the triangle law for crystal growth. [29,30]

$$B^0 = 3.85\ \rho_{Sd}^{0.5}\ G^{2.06} \qquad \text{Eqn. 20}$$

$$\Delta = 3\ G\ \tau\ \lambda_S 0.3 \qquad \text{Eqn. 21}$$

$$\rho_{Sd} = \lambda'\ \rho_c\ \lambda_s\ (G\tau)^4 \qquad \text{Eqn. 22}$$

$$\lambda_S = \frac{\rho_{sd}}{\lambda'\ B\ \rho_C G^3 \tau^4} \qquad \text{Eqn. 23}$$

Where the residence time was given by

$$\tau = \frac{V}{Q}$$ Eqn. 24

3. Materials and Methods:

At the very outset, performance modeling was undertaken to identify the key governing factors like membrane module selection, design considerations like pressure drop vis-à-vis axial distance, etc. Based on the performance modeling data, further modeling was undertaken to optimize operational parameters for the membrane crystallizer. Subsequently, the trends obtained were validated by detailed experimentation.

After the model validations, a detailed experimental study was conducted to assess the potential of MCr as a sustainable technology solution and also on the integration of the former with conventional evaporative crystallization. Figure 2 presents the schematic representation of the workflow. Artificial Neural Network (ANN) modelling was also undertaken to understand the interdependence of input and output parameters (details are provided in the supplementary material)

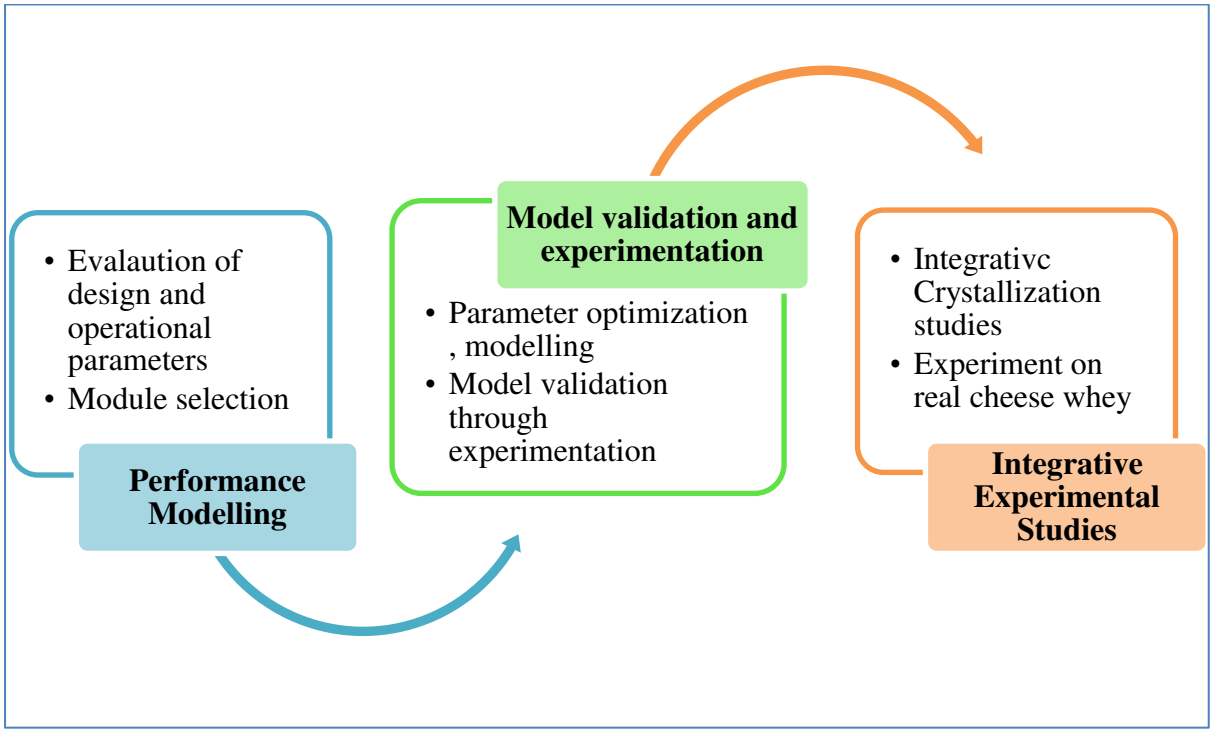

Fig.2. Schematic representation of modeling and experimental studies

For the experimental studies, all the chemicals used were of analytical grade. The chemicals were procured from Merck Chemicals, India. Initially simulated whey (without protein and lipid contents) and model lactose solutions synthesized in the laboratory was used as feedstocks. Thereafter, real cheese whey was used. The membrane used for UF was a polyethersulfone HF bundle, procured from local suppliers. The flat sheet spiral wound membranes used were simulated using the properties comparative with its HF counterpart. This helped to quantitatively compare the output flux. The Molecular Weight Cut Off (MWCO) for the membrane assembly was 100 KDa. Flat sheet NF membranes were procured from Synder Filtration. For evaluation of integrative crystallization, dewatering based UF was carried out to reach a target concentration; followed by conventional evaporative crystallization. The evaporative crystallization was carried out in a temperature-controlled hot plate.

A schematic diagram of the experimental setup is shown below in Figure 3a

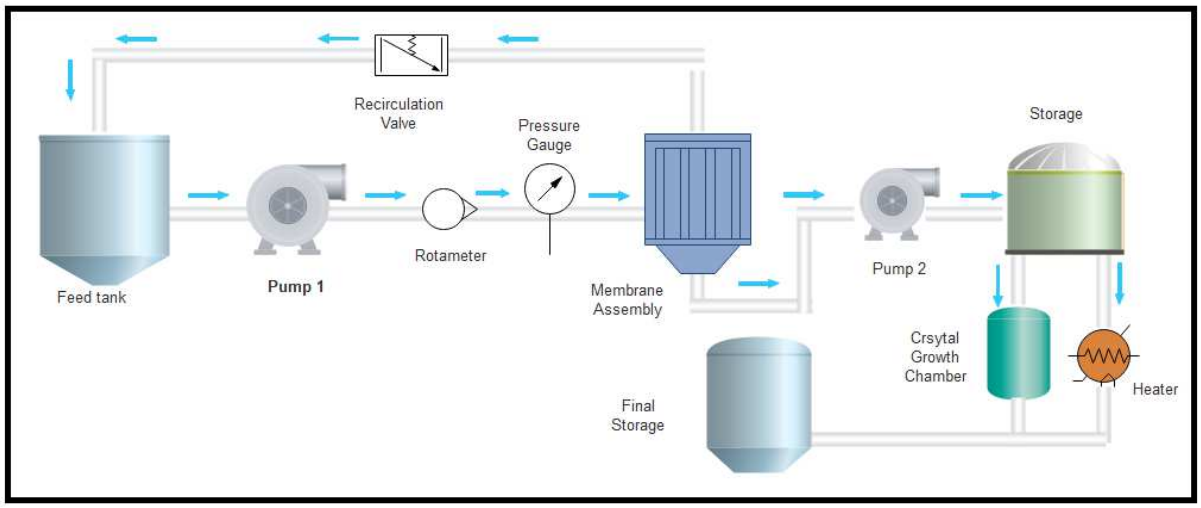

Fig.3a. Schematic Diagram of the experimental setup.

After each operational cycle, the membrane modules were backwashed with water to remove any solute buildup. Chemical cleaning with hypo was also administered to minimize the problem of concentration polarization. Standard statistical methods were used to analyze the model fits. Lactose concentration was analyzed by the standard Benedicts solution method

[31,32]. Simultaneously, the specific gravity of the solution was measured to correlate changes in concentration.

Cheese Whey Collection

Fig. 3b.Collected cheese whey, crystallization stages and extracted lactose from cheese whey.

Cheese whey was collected from local sweetmeat shops. The collected whey was preserved at 4-degree Celsius temperature to prevent any degradation. The whey was filtered to remove impurities. Subsequently, it was centrifuged at 3000 rpm for 30 minutes to 1 hour. This helped in the separation of the lipid content. Thereafter, the filtered whey was chemically treated for ammonium sulfate and/or zinc acetate for precipitation of the protein content. This was then subjected to integrated MCr for preferential crystallization of lactose. Studies were undertaken to evaluate the efficacy of integrative crystallization combining novel separation and evaporative crystallization. Changes observed in the collected cheese whey during different stages of crystallization and extracted lactose from cheese whey are shown in Figure 3b.

4. Crystal Characterization: XRD analysis

X-ray Diffraction (XRD) analysis was performed using an X-ray diffractometer (XRD) with expert system Guidance software (Model: SmartLab X-ray Diffractometer; Make: Rigaku, Japan). The X-ray diffractograms of the crystal obtained from cheese whey with integrated MCr is shown in figure 5 below:

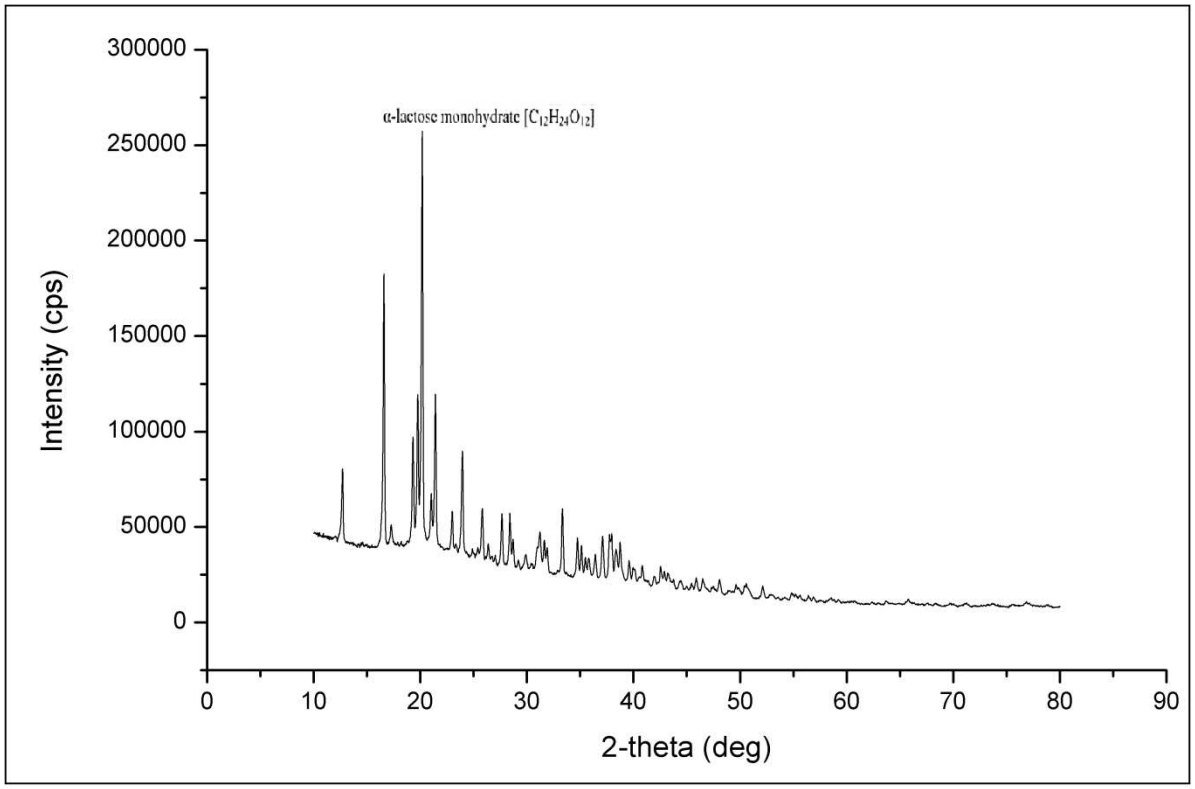

Fig.5. X-Ray Diffractogram of crystals obtained from real cheese whey

This particular experiment included integrative concentrative MCr with UF. The major phase detected in the XRD peak list is alpha lactose monohydrate. Almost similar XRD profiles were obtained for all the integrative MCr processes with a predominant presence of alpha lactose monohydrate. However, the sylvine phase of KCl was also detected in minor quantities in the crystal matrix. But overall the XRD spectra points to a reasonable pure crystal composition.

5. Results and discussions

5.1 Modelling trends:

5.1.1 Evaluation of pressure drop and mass transfer coefficient

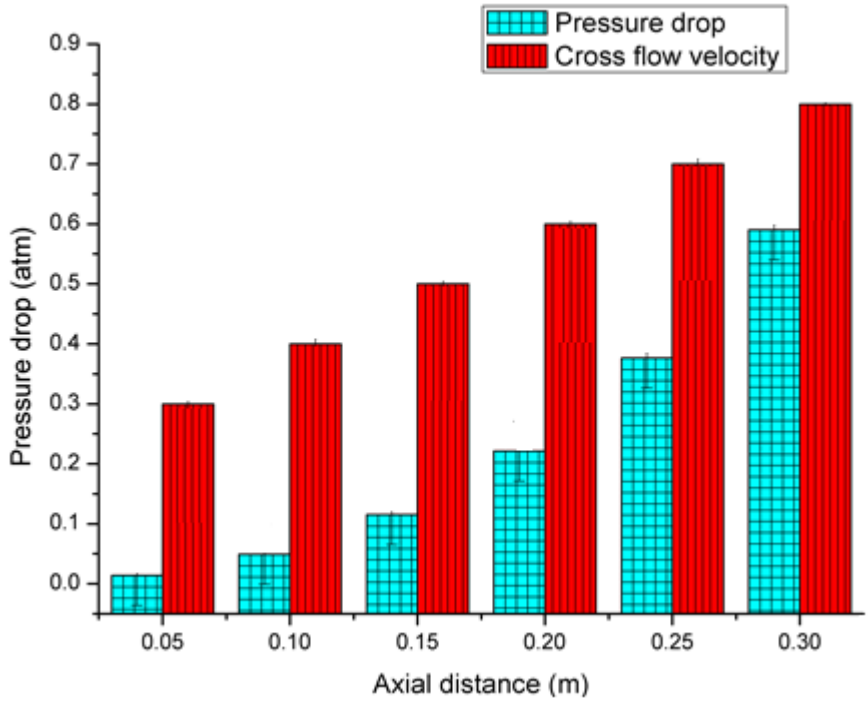

Fig. 7a. Effect of axial distance and cross-flow velocity on pressure drop

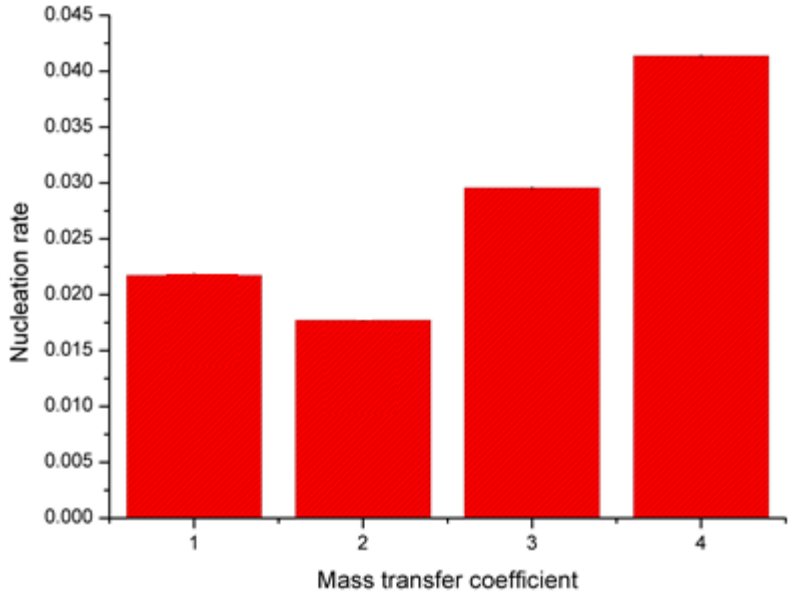

Fig. 7b. Effect of mass transfer coefficient on the rate of nucleation.

Figure 7a demonstrates the modelling trends of the pressure drop as a function of axial distance and cross-flow velocity. It was observed that pressure drop increases along the axial length of

the HF as we move from the feeding end to the exit points. This leads to a decrement of the overall driving force between the entrance and exit sections. The longer the length of a fibre bundles; the more pronounced is pressure drop. Crossflow velocity has a similar influence on the pressure drop [33]. The viscous component of the friction is responsible for the drag effect [34]. The combined effects of friction, radius, wall thickness, fluid velocity, concentration add to the retardation of the net driving force. However, a particular value of cross-flow velocity is also needed to maintain a sustained flow rate. Therefore a trade-off exists which needs to be balanced.

The reverse trend is seen in the nucleation rate variation (Figure 7b). Here as the mass transfer coefficient increases (enhanced mass transport rates), the rate of nucleation rate increases. In a solution, there is perpetual assimilation and dissimilation of aggregates. Only those aggregates grow spontaneously into nuclei which are able to overcome the required activation barrier. The membrane by providing a contact surface aids in the process of heterogeneous nucleation by lowering the energy barrier. As the rate of mass transport increases the system gradually reaches close to the supersaturation state which enhances the rate of nuclei formation. But at higher rates of mass transfer (as elucidated by the graph), the probability of molecular agglomeration increases. This is manifested in the higher mass transfer rates.

5.1.2. Performance comparison between hollow fibre and spiral wound membrane modules :

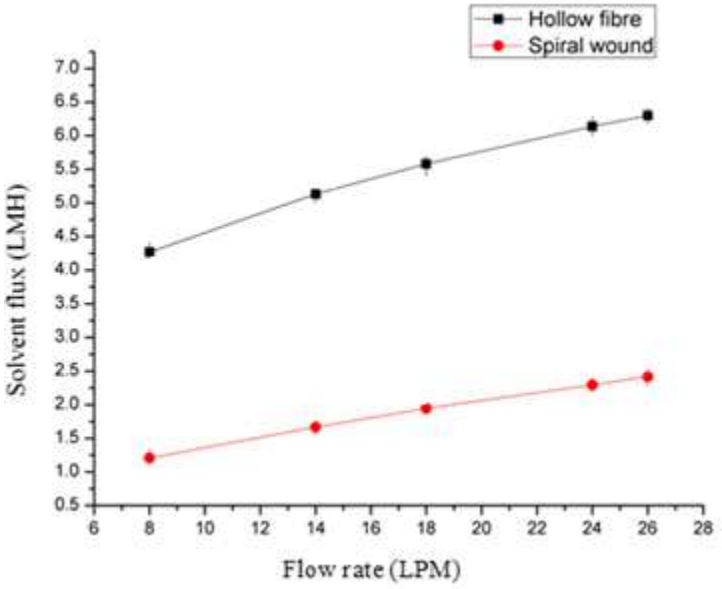

Fig. 8a. Comparison of solvent flux as a function of flow rate

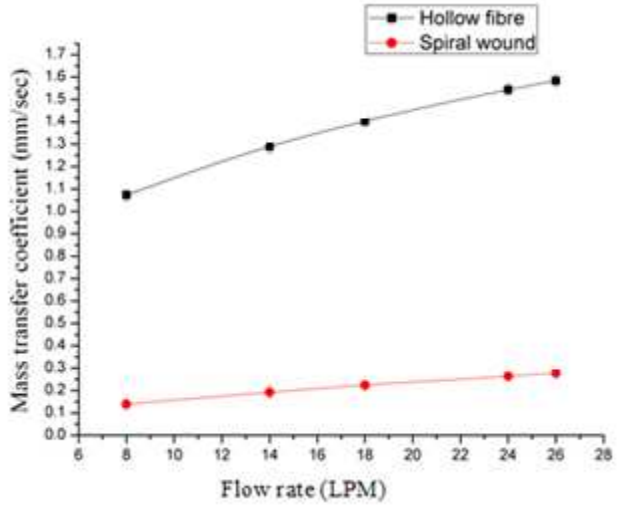

Fig. 8b. Comparison of mass transfer coefficient as a function of flow rate

The relative performance of HF and spiral wound modules was modelled to aid in membrane module selection during the experiments. The results obtained from modelling are shown in figures 8a and 8b. The solvent flux and the mass transfer coefficient of the HF modules were higher in comparison to the spiral wound counterparts. While the latter rolls a significant amount of flat sheet membrane area, it suffers from limitations of pressure drop beyond a specified number of turns on the mounted structural framework. The HF on the contrary packs a large number of thin capillary-like membranes in a small parking area. This high packing

density increases the surface area, resulting in higher mass transport. This is established in the higher mass transfer coefficient values. Consequently, the separation flux from the HF modules is higher.

At the heart of the system, is a bunch of thin capillary-like membranes arranged in a cluster. Each capillary (similar to a drinking straw) can be assumed to be an isolated shell and tube type arrangement with one central passage and multiple tiny pores on the transverse wall. Figure 8c schematically depicts such a system where the assembly acts like a bunch of shell and tube type arrangement analogous to shell and tube heat exchangers, packing a large surface area per unit volume. This enhances the mass transport and also effectively concentrates the feed by pressurized dewatering.

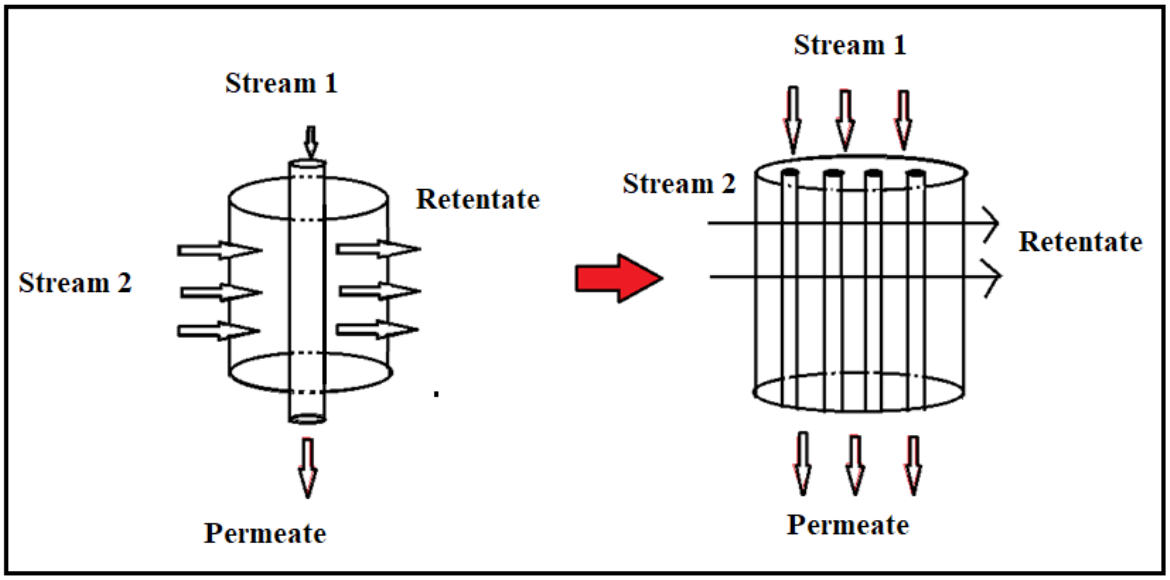

Fig.8c. Schematic diagram of a HF membrane system

The main advantage of using this HF membrane bunch is the high surface area coupled with the high packing density [35]. The fundamental driving force is provided by external pressure which causes dewatering of the solvent while the solute is preferentially retained by the membrane [36,37]. Also depending upon the process requirement, a multipass system can be operated in the same setup without the necessity of any additional components.

5.2. Modelling trends validated by experimental studies

5.2.1.Effect of feed volume variation on solvent flux

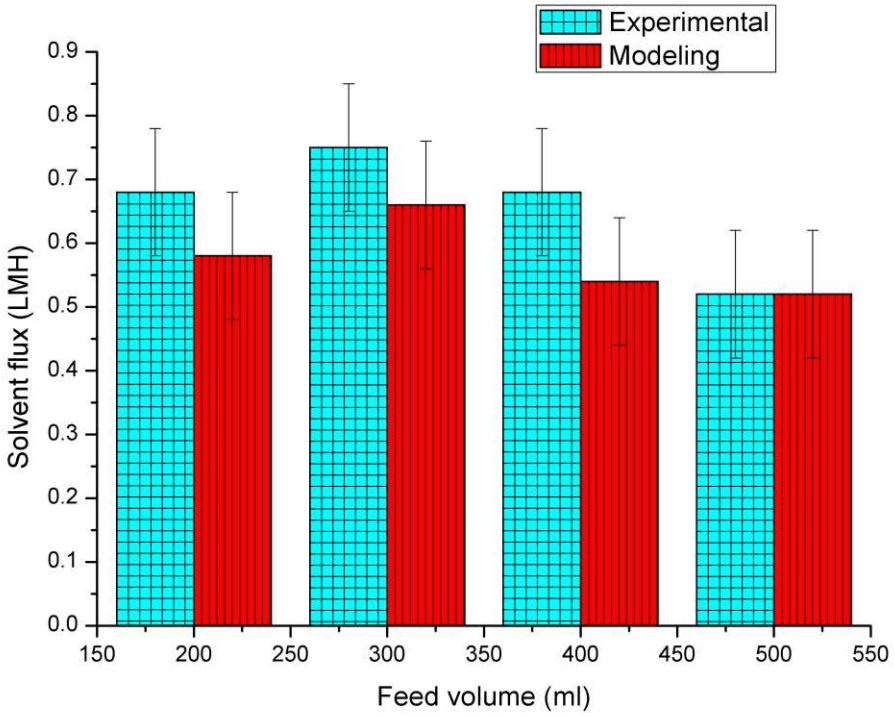

Fig.9a. Effect of feed volume variation on solvent flux (LMH)

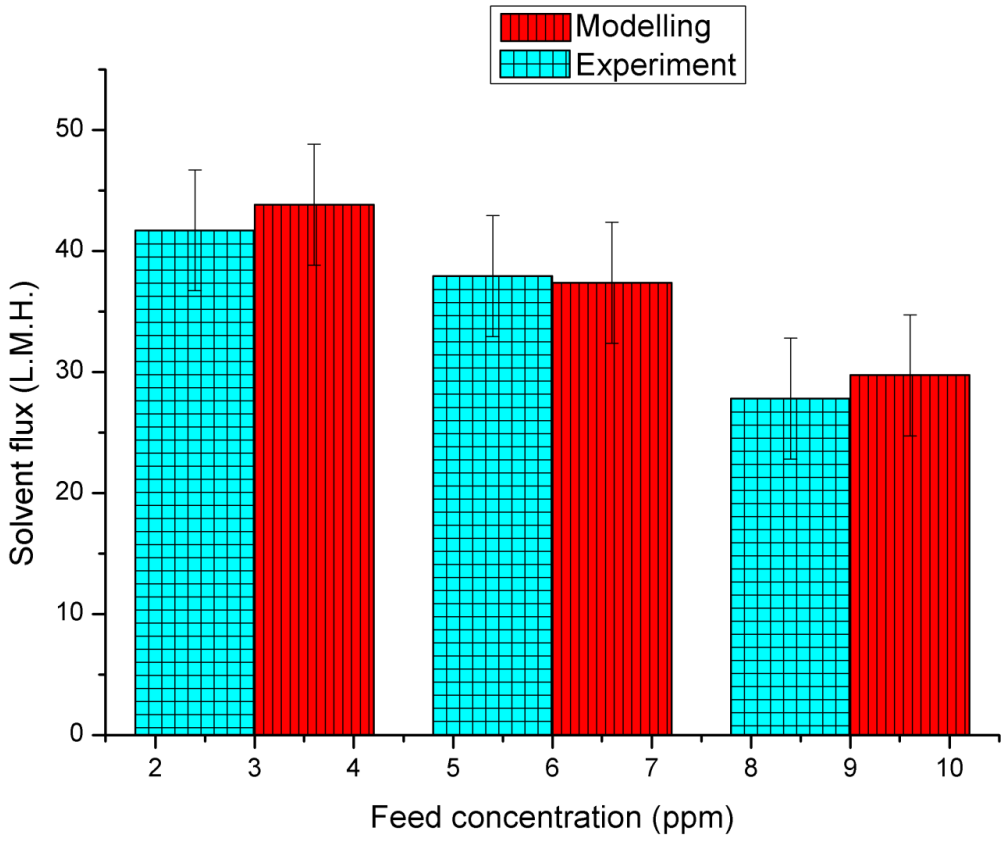

Fig.9b Effect of feed concentration on solvent flux.

Figure 9a demonstrates the effect of feed volume on the solvent flux. The feed volume was varied keeping the feed concentration constant for providing an equal basis for comparison. The incremental modelling trends were corroborated by experimentally obtained values. The solvent flux is a function of the quantity of the total feed handled as well as the driving force. For the same driving force, higher amounts of feed tend to yield higher convective mass transport rates through the membrane. This increases the solvent flux values. However, the increase in flux is not geometric as is evident from the trend lines. Under the same operating conditions and TMP, beyond a certain point, the curve tends to become asymptotic.

Variation in feed concentrations and their effect on the solvent flux was evaluated as shown in Figure 9b above. The feed volume handled, TMP, flow rate, were kept constant. The experiment was run in semi-continuous mode and was continued till the entire feed solution present in the feed chamber was dewatered. The run times were kept in the range of 2-5 minutes

and constant time cycles were maintained for every set of experiments. The experimental datasets corroborate the model predicted downward trend of solvent flux with an increase in the concentration of the feed. At increased solute concentration, the dewatering rate diminishes. At constant pressure and flow rate, with an increase in the bulk feed concentration, solute accumulation at the membrane interface increases. This leads to the creation of concentration gradients between the bulk and interface. An additional mass transfer resistance is also imposed due to the solute accumulation at the boundary layers. The mass transfer coefficient decreases leading to lower water transport rates and hence lower solvent fluxes are obtained.

5.2.2. Effect of pressure and flow rate on solvent and solute flux

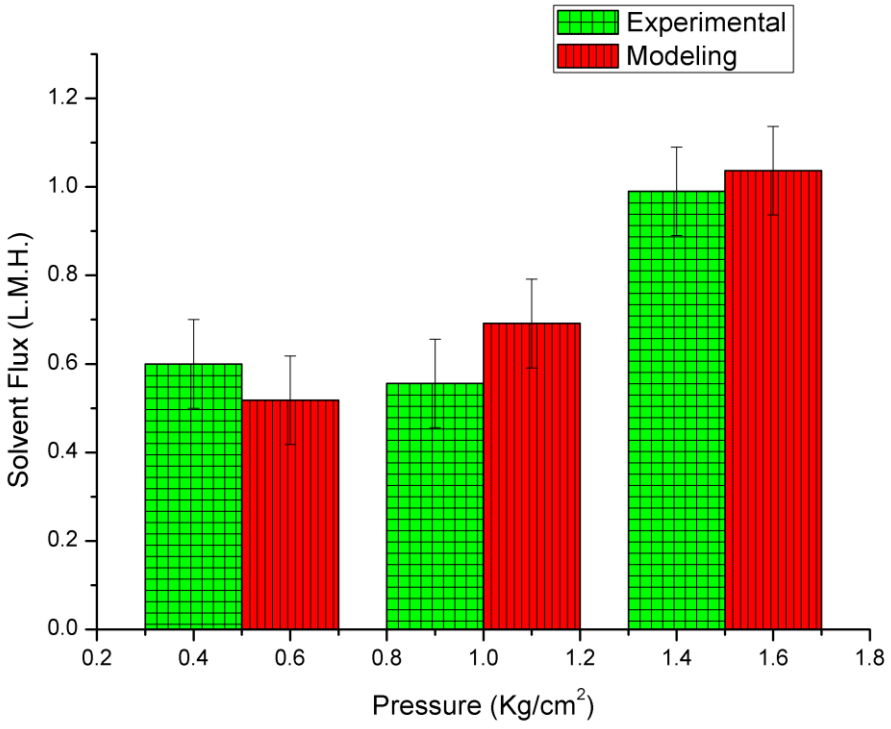

Fig.10a. Variation of solvent flux with pressure

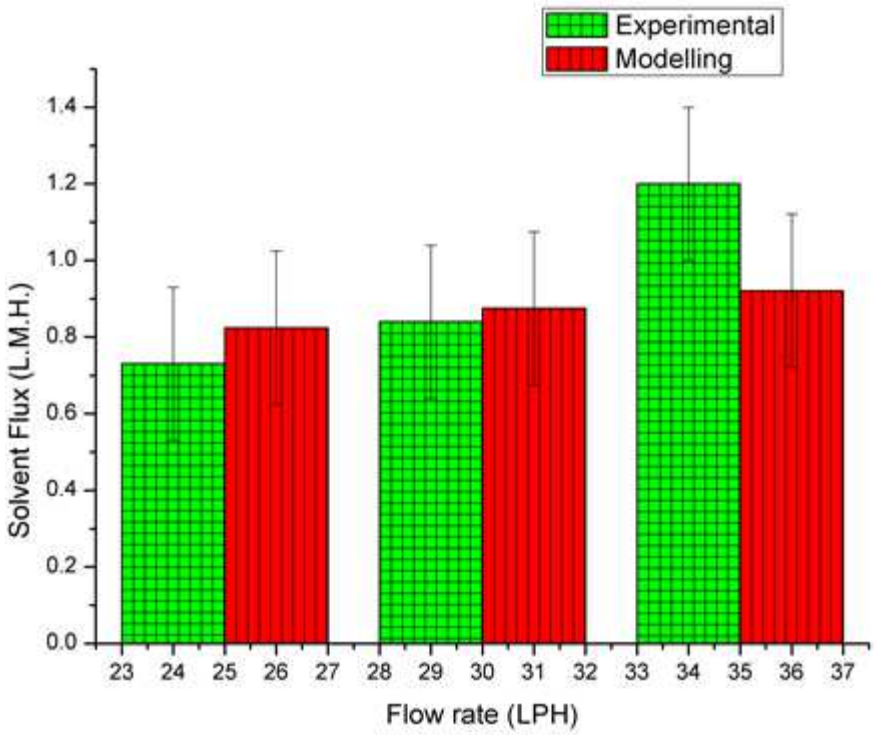

Fig.10b. Variation of solvent flux with flow rate

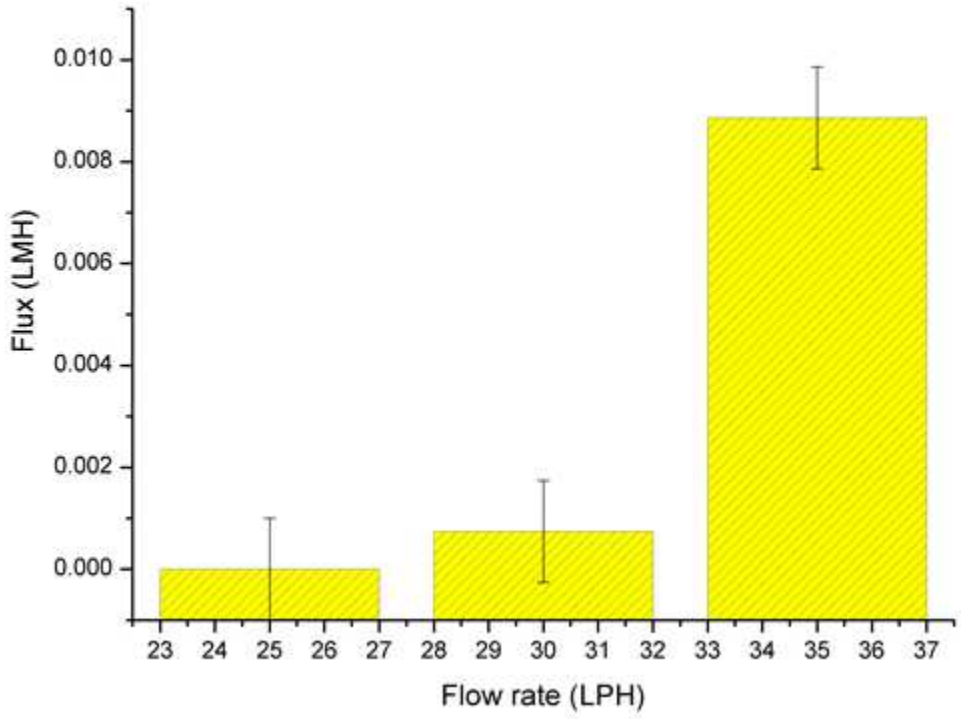

Fig.10c. Effect of flow rate on solute flux

The effect of external pressure on solvent flux was evaluated experimentally and by modelling. The comparative results obtained from modelling vis-à-vis experimental validation are shown in figure 10a. The TMP was varied in the range of 0.5 - 1.5 kg/cm^2. The total time of operation was in the range of 2-5 minutes with a constant time maintained for each set of pressure variations.

UF membrane is effective in retaining macromolecular solutes; this leads to high solute rejection and consequent high solvent flux. Ideally, for a fixed set of membrane characteristics and MWCO value, the flux increases with an increase in the TMP as is obtained from the modelling trend. However a slight deviation between the experimentally obtained curve and the modelling trends. The probable explanations for this could be membrane fouling or decay in flux values. The solvent flux provides a direct estimation of the dewatering rate from the process at a rate roughly equivalent to the solvent flux. The energy consumption for dewatering by way of application of external pressure is commensurately lesser than the equivalent energy needed to evaporate the same amount of solvent. Also important is to consider the total run time of the operation. The short duration of the total operation points to the efficiency of the membrane in dewatering the feed.

The effect of the cross-flow rate on the solvent was modelled as well as evaluated experimentally. The comparative results are depicted in Figure 10b. The corresponding solute flux was also estimated by calculating the permeate concentration from the experimental results (Figure 10c). Both the modelling and experimental trends show an increasing trend of solvent with an increase in flow rate. The first reason is the increase in the volume of feed that is processed through the membrane. There is also the additional effect of the cross-flow rate which generates a sweeping force over the membrane surface due to its tangential flow through it. This also drives away any solute buildup on the membrane surface leading to a gradual

increase in the throughput through the membrane. The solvent flux versus flow rate is also critical for understanding the rejection through the membrane. As the permeate volume increases, for a fixed bulk concentration and flow rate, the solute concentration increases. But owing to a high rejection, the magnitude of solute flux is negligible. Hence there is less solute loss. The experimental trends corroborate the modelling results. Previous studies conducted have also shown that as the flow rate increases, there is a gradual increase in the solvent flux [38].

5.3 Experiments towards integration of MCr with evaporative crystallization

5.3.1 Variation of solvent flux with operational time

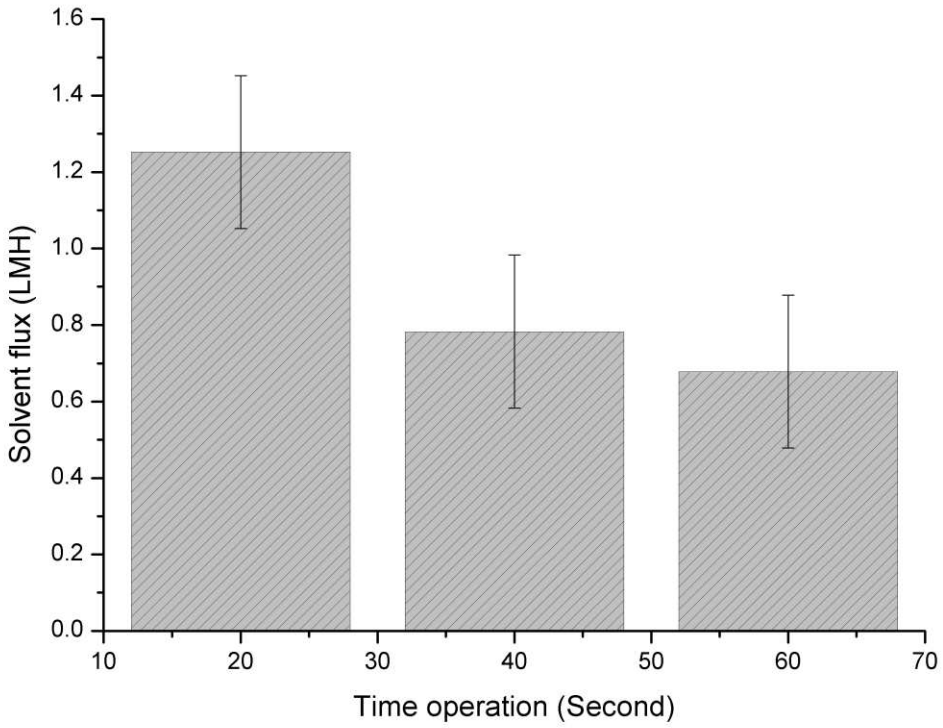

Fig.11 Change in solvent flux with time

The experimental results of variation of solvent flux with time are displayed in figure 11. The feed concentration was kept constant for all set of operational time-varying experiments. The TMP was also kept constant at 1.5 kgf/cm^2. The cross-flow rate through the membrane was

maintained in the constant range of 25-30 Litres per Hour (LPH). The data was recorded for one-pass operation through the HF membrane module. The mode of operation was semi-continuous and the operational time range was varied such that for a single pass of operation, the feed present in the feed chamber was completely dewatered. The flow rate and associated parameters were also optimized accordingly.

The solvent flux data presents a declining trend with respect to time. This is due to the concentration gradient established between bulk feed and feed-membrane interface leading to a concentration boundary layer formation. However, its effect is not pronounced on overall flux values, owing to the sweeping force generated by the tangential flow of feed. Nevertheless, the solvent flux decreases with time. There is also the probability of membrane fouling. Here the feed material is organic and suffers from a high propensity to foul the membranes [39]. This declining trend published in numerous studies [40,41] establishes one of the drawbacks of membrane-based separation. However, with backflushing and chemical dosing this can be remediated to a large extent and the operational life of a membrane can be enhanced.

5.3.2 Variation of retentate concentration per pass of ultrafiltration

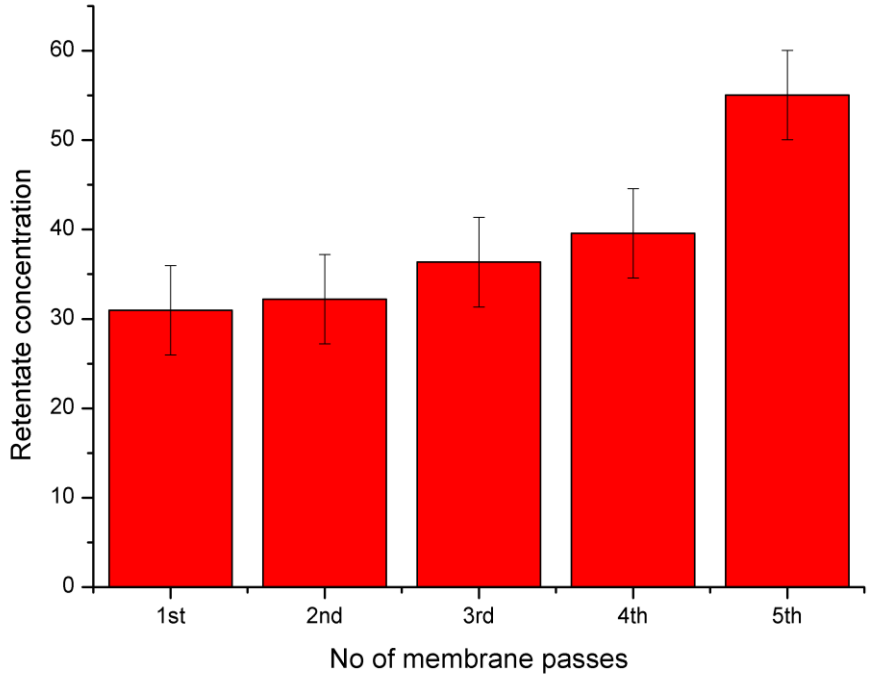

Fig.12. Retentate concentration after different passes of UF

Effect of the passage of solvent in a multi-pass configuration with respect to retentate stream concentration was studied experimentally (figure 12). The aim was to evaluate the dewatering potential of the UF membrane as a function of membrane pass and feed concentration. Lactose solution with an initial concentration of 10g/lit was the feedstock. The TMP was kept at 0.25 kg/cm^2 while the crossflow rate was maintained in the range of 12-15 LPH. The membrane separation was undertaken at ambient temperature. Each pass through the membrane was carried out till the entire feed volume was dewatered. The same feed was subjected to UF till the complete feed was dewatered in one cycle. Subsequently, the retentate stream collected from that pass was taken to the feed chamber. Hence for the next cycle, the retentate from the previous pass became the feed. A small fraction of solute is lost during every pass which is present in the permeate stream as the practical rejection by the membrane is not 100%. The gradual increase in retentate concentration indicates a progressive concentration of the feed

which is the main property that is utilized in membrane-based filtration. The concentration by the membrane occurs at room temperature which points to the utility of the process. However, the feed concentration attained by the membrane does not increase indefinitely. Nevertheless, this property may be utilized in designing compact setups that can be used as a multipass unit for feed concentration to near supersaturation concentrations. However, it is important to note that, as the number of membrane passes increase, the energy consumption incurred during the operation also increases.

5.3.3 Effect of crystallization time in the presence and absence of membranes

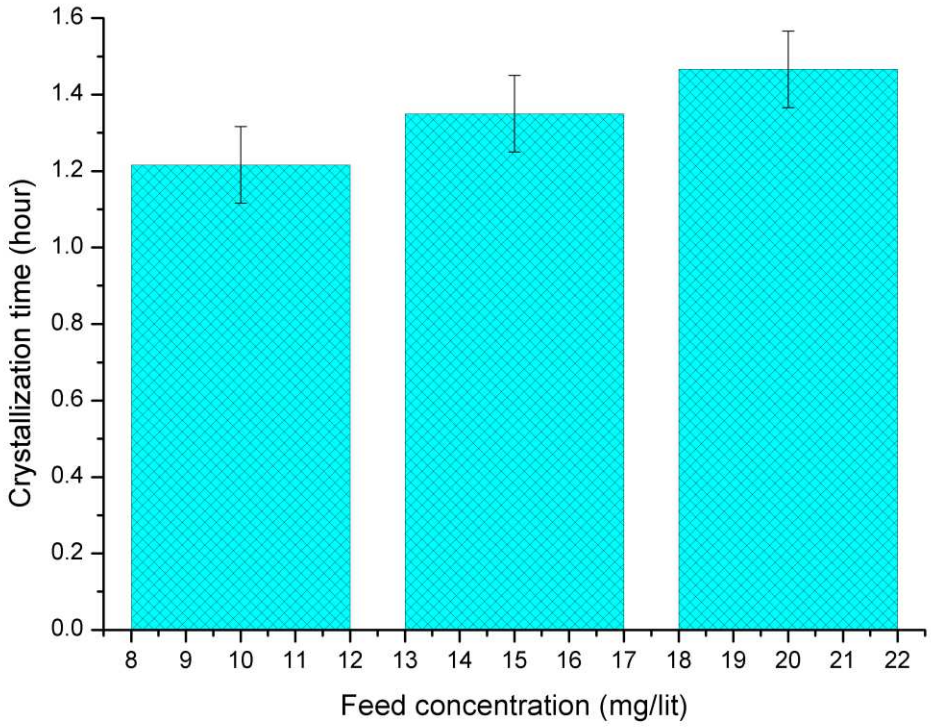

Fig.13a. Effect of feed concentration on crystallization time in the presence of membrane

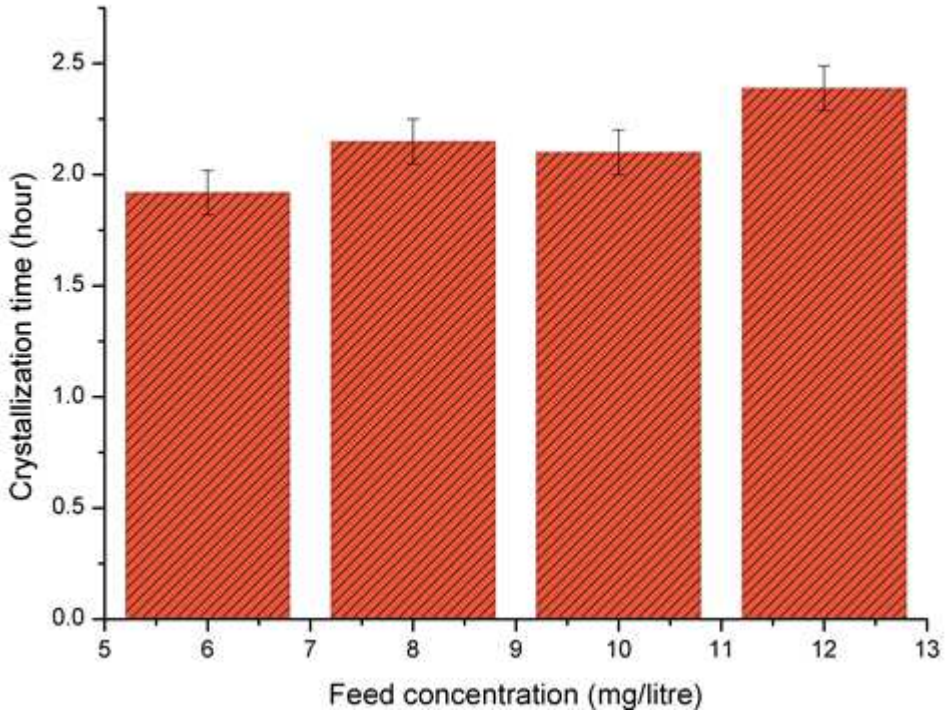

Fig.13b. Effect of feed concentration on crystallization time in the absence of membrane

Effect of feed concentration on crystallization time in the presence and absence of membrane was studied (Figure 13a and 13b respectively). The key rationale behind the study was to evaluate effect of the membrane on the potential lowering of crystallization time and to assess the possibility of integration of evaporative crystallization with MCr all the operations where the system was subjected to 3 pass UF. Thereafter the volume of the retentate was varied and the crystallization was completed through evaporative means. For the same concentration, as the volume of the solution increases, the time needed to attain crystallization increases since the heating rate is also kept constant. Therefore, at the same evaporation rate, the solution with a higher volume takes longer to reach the supersaturated state. The presence of the membrane shows a marked influence on the crystallization time. There is a 25-30% reduction in the time of crystallization. The retentate obtained was at a higher concentration and consequently, the crystallization time was lower by around an hour. This also leads to a commensurate amount of energy savings after including the energy required to operate the membrane setup. Also, a possible combination of the two processes could aid in cutting down crystallization time and

total energy consumption. Another potential benefit of lower crystallization time is the prevention of possible heat degradation for thermally sensitive feedstocks.

5.3.4 Variation of feed volume and time in evaporative crystallization

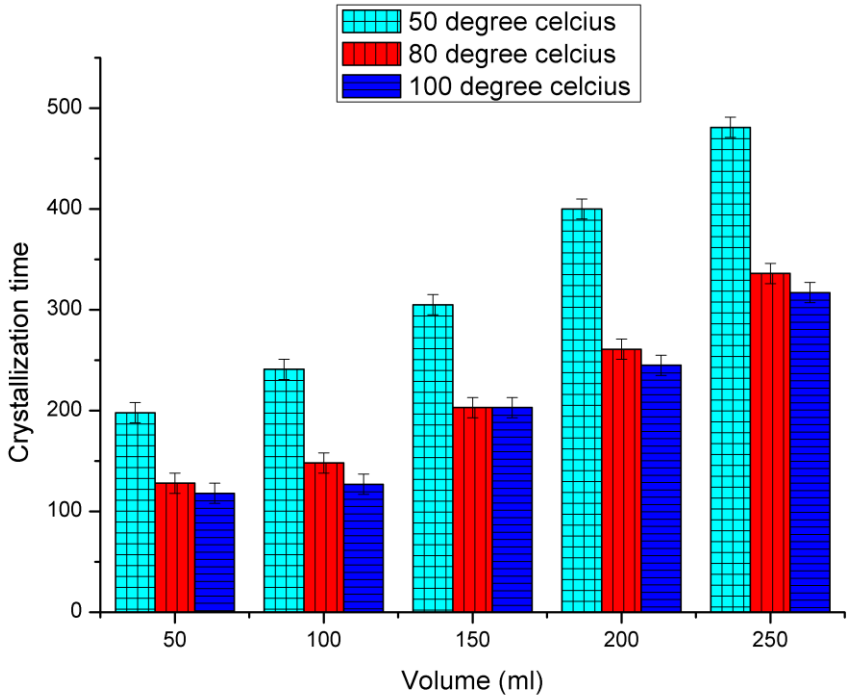

Fig.14a. Variation of crystallization time with feed volume and temperature

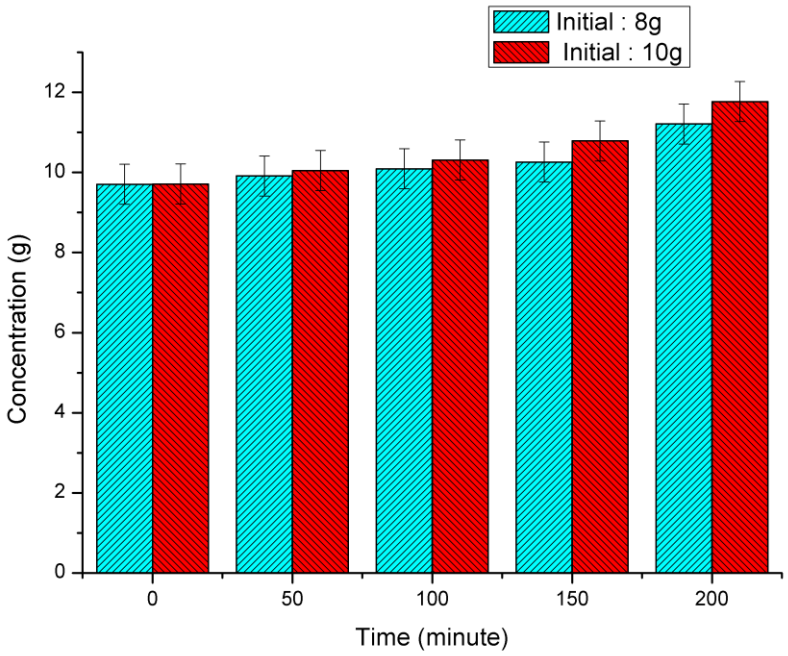

Fig.14b. Effect of time variation on the final concentration

Effect of feed volume on crystallization time and the effect of time on final concentration were studied experimentally. Figures 14a and 14b illustrate the results. Direct evaporative crystallization was used to study the effect of volume variation. The feed concentration was kept constant for all the experiments. The same rate of heating was maintained for all the solutions to provide an equal basis for comparison.

Initially, the effect of volume variation was studied. The effect of temperature on crystallization was also studied concurrently by heating the feeds at different temperatures. At the same feed concentration, the solution with a higher feed volume demonstrates a higher crystallization time. As the temperature is increased the time taken for crystallization diminishes as the evaporation rate becomes faster at higher temperatures. This holds for the corresponding crystallization times of solution of different volumes. From the data, it is seen that both feedstocks become potentially more concentrated over time. However, the difference in the final concentrations between the two feedstocks increases with time. The effect of evaporative concentration as a function of temperature, feed volume and concentration show trade-offs that

need to be addressed carefully for optimum efficiency and process integration.

Figure 14b demonstrates changes in feed concentration with time during evaporative crystallization. Feedstocks of two different concentrations were subjected to evaporative crystallization at the same heating rate. This was done to evaluate the concentration attained at different stages of evaporative crystallization. This will help ascertain the possibility of a combination of conventional evaporative crystallization with membrane-based concentrative crystallization.

5.3.5 Experiments on real cheese whey: role of antisolvent addition on integrated MCr process

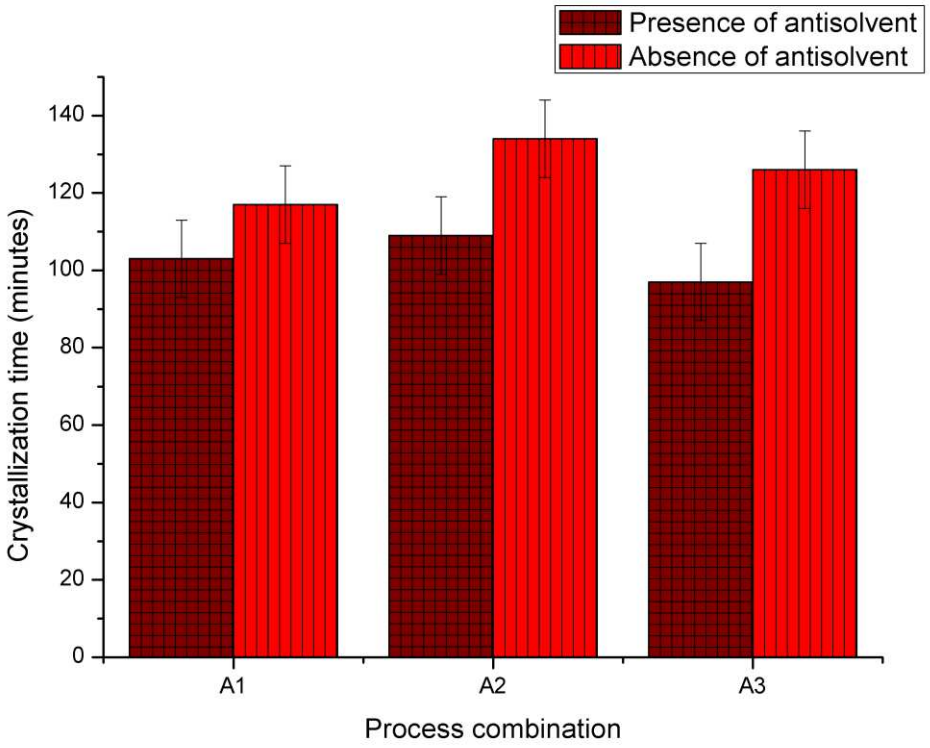

Fig. 15a. Effect on Antisolvent addition on integrated MCr and chemical precipitation processes

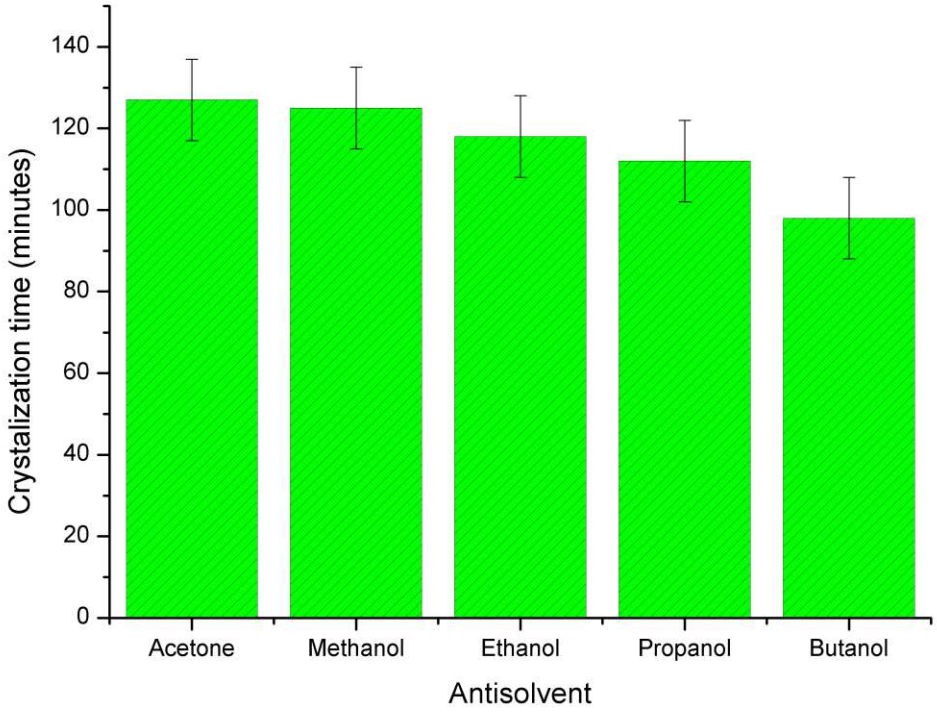

Fig.15b. Effect of nature of antisolvent on crystallization time

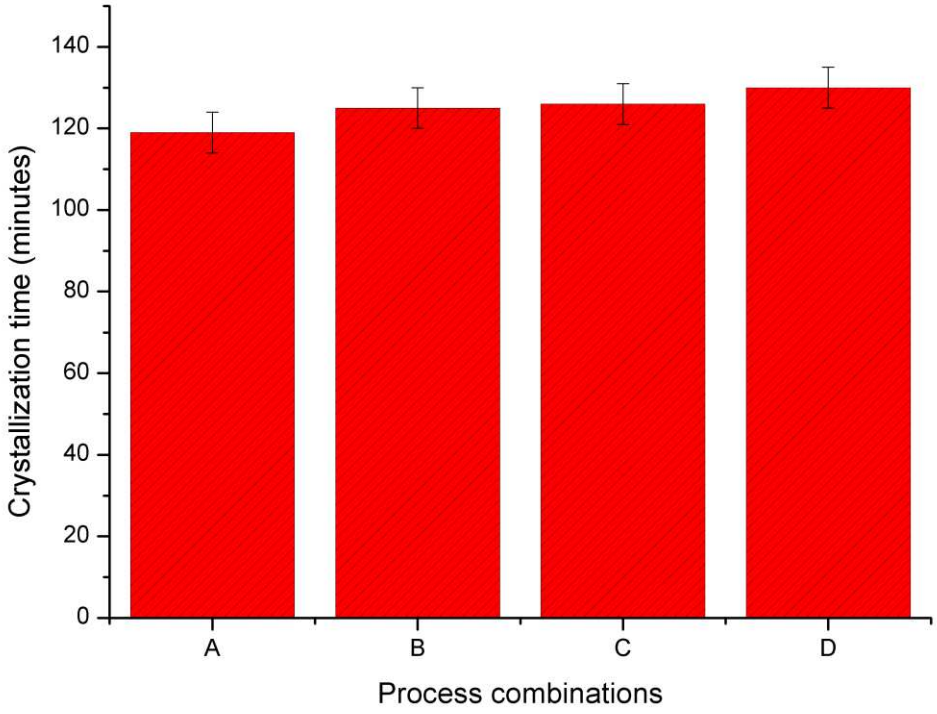

Fig.15c. Effect of different integrated MCr on crystallization times

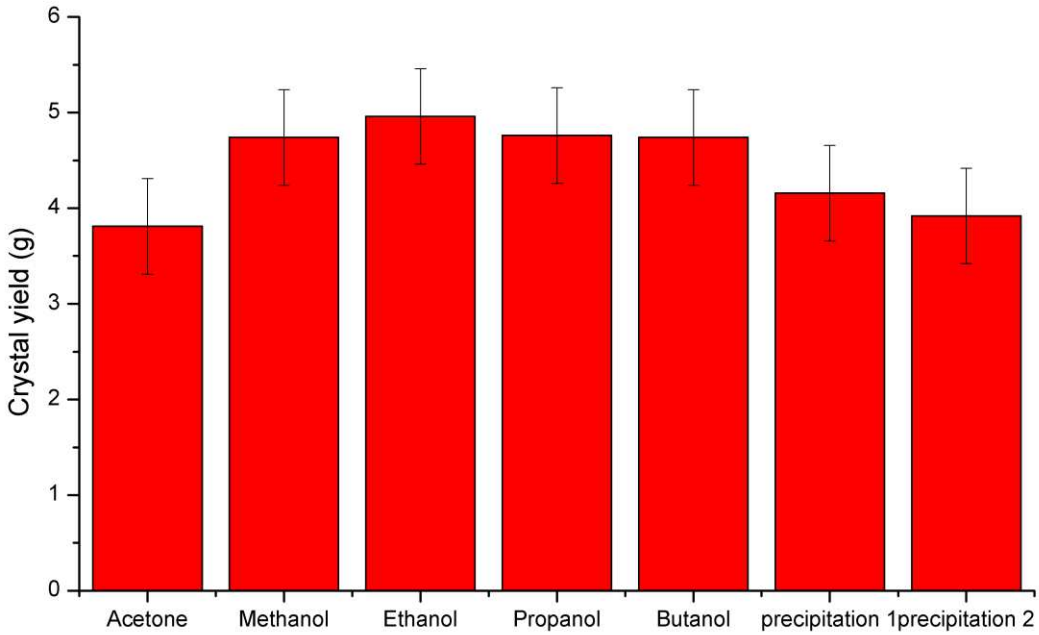

Fig.15d. Crystal yields obtained from different integrated MCr approaches

Experimental results of lactose extraction from real whey are presented in the figures 15a to 15d above. Different integrative experiments were conducted to assess the efficiency and feasibility of the membrane integrated crystallization techniques for lactose recovery. Efficacy of chemical precipitation techniques like zinc acetate addition and/or ammonium sulfate towards lactose extraction was studied. Simultaneously, the effect of antisolvent addition on lactose extraction and its subsequent precipitation/crystallization was also calculated.

Process combinations in figure 15a: viz, A1, A2 and A3 represent chemical precipitation processes consisting of zinc acetate addition, addition of ammonium sulfate and a combination of zinc acetate and ammonium sulfate addition respectively. Lactose crystallization using the aforesaid process combinations were undertaken in the presence and absence of antisolvent. The same quantity of antisolvent was used for all the experiments for an equal basis of comparison (in this case acetone was the antisolvent).

In the next figure 15b, different chemical precipitation experiments were studied. For this set of experiments, no antisolvent was added.

Process combinations A, B, C, D represent the following:

A: integrated zinc acetate addition and cross-flow Nanofiltration

B: integrated ammonium sulfate addition and cross-flow NF.

C: integrated zinc acetate addition and cross-flow UF.

D: integrated ammonium sulfate addition and UF.

In terms of the total time for crystallization, the addition of antisolvent has shown a marked decrease in the crystallization times. In the chemical precipitation experiments, antisolvent addition has caused 13.59% reduction (combination A), 22.94% reduction (combination B), and 23.01% reduction (combination C) in the crystallization times for the process. Antisolvent crystallization is a sustainable alternative as compared to energy-intensive evaporative crystallization. The lower crystallization times are particularly significant for biodegradable feedstocks sensitive to pressure and temperature variations in the solution. Antisolvents decrease the solubility of lactose in water promoting a higher degree of lactose-lactose interaction. This increases the selective cohesion among the lactose molecules and gradual separation of the lactose [42].

Among the antisolvents in the alcohol series, the higher alcohols tend to show a greater reduction in the crystallization times (figure 15c). There is a general decrease in the solubility/ miscibility of the alcohols with an increase in the molecular weights [43]. There is also a corresponding increase in the hydrophobicity of the antisolvents in the alcohol series from methanol to propanol. This enhances the adhesive interactions between lactose and the water molecules, leading to faster separation of the lactose from the medium [44]. This is manifested in the lowering of the crystallization times.

For the integrated MCr - chemical precipitation processes, cross-flow NF demonstrated shorter crystallization duration as compared to cross-flow UF. This is due to the higher degree of feed concentration in crossflow NF. The TMP of NF is higher than UF, and the degree of rejection obtained in the process of NF is higher as compared to UF. The data of higher concentration of lactose in the membrane rejects of cross-flow NF is also corroborated by the literature [45, 46]. Lactose being a macromolecular feedstock, UF also demonstrates competitive lactose retention. However, the total energy consumption in the process of NF is higher than UF due to the higher driving force requirements. Hence, there is a trade-off that

exists between crystallization time and energy consumption which needs to be addressed in the process selection.

Lactose crystal yields from different crystallization experiments are presented in figure 15d. The experiments were conducted with similar batches of 100ml solutions. The lactose yield was obtained after protein and fat content from the cheese whey was removed. The density of the residual whey comprising primarily of lactose fractions was estimated at 0.48 g/cc. The composition and purity of the lactose crystals extracted from cheese whey have been ascertained by XRD analysis (presented in section 4 above). Highest lactose crystal yields were observed in the process combinations involving antisolvent addition. The yields varied in the range of 3.8g to 4.46g per 100ml of deproteinated cheese whey.

The addition of alcohol as antisolvents demonstrated a lowering of crystallization times. Among the alcohol molecules used as antisolvents, the crystal yield increased on progression in the alcohol series. This is also congruent to the relatively faster crystallization times obtained in the alcohols series.

6. Error Analysis:

Error analysis was carried out to evaluate the model fit. Standard error analysis procedures were followed.

Root mean square error (RMSE) was computed using the following equation

$$RMSE = \left(\sum_{i=1}^{p} \frac{(X_i - Y_i)^2}{p} \right)^{1/2}$$

From the RMSE values, the Relative Error (RE) was also calculated $RMSE = RE/EXP_{mean}$

Where EXP_{mean} is the average of the corresponding experimental values

The calculations are tabulated in table 1

Table 1 : RMSE and RE values of the model fits

variation	RMSE	RE
flux vs pressure	0.095	0.132
flux vs flow rate	0.171	0.1854
flux vs volume	0.0989	0.15

From table 1 , the low RMSE and RE values indicate a good model fit when the model results were validated by experiments.

7. **Conclusion and Future Work**

The following conclusions can be drawn from the study:

(i) Preferential extraction of lactose from cheese whey produced competitive crystal yields in the range of 3. 8- 4.96g per 100 ml of deproteinated whey with membrane integrated anti-solvent crystallization.

(ii) The addition of antisolvent showed a marked influence on the crystallization time. When anti-solvent from the alcohol series is used, there is a gradual lowering of crystallization time from methanol to butanol.

(iii) MCr demonstrated 25-30% reduction in the crystallization times as compared to standalone evaporative crystallization. The addition of antisolvents also led to further crystallization time reduction in the range of 13.6% - 23.1% when used in the conjunction with MCr and chemical precipitation experiments.

(iv) Stagewise concentrative mode of MCr was successful in concentrating feedstocks. But increasing the no. of membrane passes beyond a particular concentration did not result in an infinite concentration increase of the feed.

(v) Among the pressure driven membrane processes employed, integrated cross flow NF demonstrated a higher feed concentration than cross-flow UF. However, energy consumption associated with NF was also higher. This led to a trade-off.

(vi)The operationally flexible MCr technique can be coupled with evaporative crystallization. This does not possess the prerequisite of scraping off the existing infrastructure, offering an advantage in the process design.

(vii) While comparing membrane module, HF membranes have established higher solvent flux and mass transfer coefficients as compared to flat sheet membranes.

(viii) The quality of lactose crystals was ascertained with wet chemical analysis and X-ray diffraction. The XRD values indicated reasonable purity of the lactose crystals extracted from cheese whey

(ix) In future, the integrated MCr techniques can be applied for value-added product recovery from other wastewater streams. Scale-up studies also need to be undertaken for large scale technology development.

8. Nomenclature

n = number of fibres

r_i = Internal radius of HF

r_o = External radius of HF

L= Length of 1 HF

ε= porosity

η= viscosity

x = Distance at a point along the length of the fibre

δ = Membrane thickness

v_f= cross flow velocity

f = flow rate

A= Area of cross-section

Sh= Sherwood number

K_1,K_2 = constants

N_{Re} = Reynolds number

ρ = density

d_i = Hydraulic diameter

D= Diffusivity

$\hat{k}$ = mass transfer coefficient

Sc= Schimdt number

S= Structural parameter

τ = tortuosity

J_v = Solvent flux

C_p= permeate concentration

C_b = bulk/ feed concentration

C_m = concentration at the membrane surface

f_D = friction factor

ΔP_i = pressure drop

Xi = Experimental results

Yi = model results

E_{mean} = Average of all experimental results

W= Module Width

D= Module Diameter

n= Number of Turns

H_f= Feed spacer thickness

Hp= Permeate spacer thickness

A_f = Feed spacer cross- sectional area

A_p= Permeate spacer cross- sectional area

K_d = Mass transfer coefficient of liquid

S^* = Supersaturation ratio

S' = Supersaturation attained

S_e = Equilibrium supersaturation

B^0 =Nucleation rate

G^* = Crystal growth rate

Q = Flow rate

ρ_{sd}= Density of crystal (from solution)

λ_s = Shape factor

λ' = constant

ρ_C = Crystal density

τ' = Induction time

9. References

1) B.K. Pramanik, K. Thangavadivel, L. Shu, V. Jegatheesan, A critical review of membrane crystallization for the purification of water and recovery of minerals, *Rev. Environ. Sci. Bio/Technol*. **15**, 2016. doi:10.1007/s11157-016-9403-0.

2) G. Wen, Z. Hu, X. Liu, L. Huang, Improvement of the quality of struvite crystals recovered from a mixture of human urine and municipal sewage via a novel two-

step precipitation method, *Environ. Technol. Innov*. **12**, 2018. doi:10.1016/j.eti.2018.08.003.

3) I. Ruiz Salmón, P. Luis, Membrane crystallization via membrane distillation, *Chem. Eng. Process*. **123**, 2018. doi:10.1016/j.cep.2017.11.017.

4) P. Das, K.K.K. Singh, S. Dutta, Insight into emerging applications of forward osmosis systems, *J. Ind. Eng. Chem.* **72,** 2019, doi:10.1016/j.jiec.2018.12.021.

5) D. Sharma, Z.V. Murthy, S.R. Patel, Microfluidic antisolvent crystallization of lactose: Effect of process parameters, *Waste and Biomass Valorization*. 2022. doi:10.1007/s12649-022-01691-3.

6) P. Das, K. Singh, Broad-spectrum contaminant removal from water using sustainable pressure assisted osmosis, *J. Environ. Chem. Eng*. **9**, 2021,. doi:10.1016/j.jece.2020.104594.

7) K.K. Sirkar, A.G. Fane, R. Wang, S.R. Wickramasinghe, Process intensification with selected membrane processes, *Chem. Eng. Process*. **87**, 2015. doi:10.1016/j.cep.2014.10.018.

8) K. Huang, H. Liu, Controllable interfacial mass transfer intensification for multi-liquid phase extraction of platinum, palladium and rhodium from Wasted Auto-catalysts, *Waste and Biomass Valorization*. **4, 619-626,** 2012. doi:10.1007/s12649-012-9168-9.

9) C. Quist-Jensen, F. Macedonio, E. Drioli, Membrane crystallization for salts recovery from brine—an experimental and theoretical analysis, *Desalin. Water Treat.* **57**, 2015 7593–7603. doi:10.1080/19443994.2015.1030110.

10) P. Das, S. Dutta, K.K. Singh, Insights into membrane crystallization: A sustainable tool for value added product recovery from effluent streams, *Sep. Purif. Technol*. **257**, 2021. doi:10.1016/j.seppur.2020.117666.

11) A. Ali, C. Quist-Jensen, F. Macedonio, E. Drioli, Application of Membrane Crystallization for Minerals' Recovery from Produced Water, *Membranes.* **5**, 2015. doi:10.3390/membranes5040772

12) P.Das, AK Singh, KKK Singh. Sustainable Technologies for Value Added Product Recovery from Wastewater. Environmental Degradation: Challenges and Strategies for Mitigation, 395-417, 2022, Springer

13) P. Tzatsi, A.M. Goula, Encapsulation of extract from unused chokeberries by spray drying, co-crystallization, and Ionic gelation, *Waste and Biomass Valorization*. 2021. doi:10.1007/s12649-020-01316-7.

14) K.D. Bhuyar, S.G. Suke, S.D. Dawande, Treatment of milk wastewater using up-flow anaerobic packed bed reactor, *Pol. J. Chem. Technol*. **17**, 2015 84–88.doi:10.1515/pjct-2015-0034.

15) E.S. Mansor, E.A. Ali, A. Shaban, Tight ultrafiltration polyethersulfone membrane for cheese whey wastewater treatment, *Chem. Eng. J.* **407,** 2021. doi:10.1016/j.cej.2020.127175.

16) R.R.D. Souza, R. Bergamasco, S.C.D. Costa, X. Feng, S.H.B. Faria, M.L. Gimenes, Recovery and purification of lactose from whey, *Chem. Eng. Process.* 49, 2010. doi:10.1016/j.cep.2010.08.015.

17) M. González-Amado, A.P. Tavares, M.G. Freire, A. Soto, O. Rodríguez, Recovery of lactose and proteins from cheese whey with poly(ethylene)glycol/sulfate aqueous two-phase systems, *Sep. Purif. Technol.* **255**, 2021. doi:10.1016/j.seppur.2020.117686.

18) R. Rossano, A. Delia, P. Riccio, One-Step Separation from Lactose: Recovery and Purification of Major Cheese-Whey Proteins by Hydroxyapatite—A Flexible Procedure Suitable for Small- and Medium-Scale Preparations, *Protein Expr. Purif.* **21**, 2001165–169. doi:10.1006/prep.2000.1350.

19) M. Kasmi, Biological processes as promoting way for both treatment and valorization of dairy industry effluents, *Waste and Biomass Valorization*. **9** , 195–209, 2016. doi:10.1007/s12649-016-9795-7.

20) X. He, F. Ren, H. Guo, W. Zhang, X. Song, B. Gan, Purification and properties of a milk-clotting enzyme produced by bacillus amyloliquefaciens D4, *Korean J Chem Eng*. **28** , 2010. doi:10.1007/s11814-010-0347-8..

21) P.I. Omwene, M. Yagcioglu, Z.B.O. Sarihan, A. Karagunduz, B. Keskinler, Recovery of succinic acid from whey fermentation broth by reactive extraction coupled with multistage processes, *J. Environ. Chem. Eng*. **8**, 2020. doi:10.1016/j.jece.2020.104216.

22) A. Fane, C. Fell, A. Waters, The relationship between membrane surface pore characteristics and flux for ultrafiltration membranes, *J. Membr. Sci*. **9**, 1981 doi:10.1016/s0376-7388(00)80267-7.

23) S. Kimura, Characterization of Ultrafiltration Membranes, *Polym. J.* **23** , 1991. 389–397. doi:10.1295/polymj.23.389.

24) J.R. Mccutcheon, M. Elimelech, Modeling water flux in forward osmosis: Implications for improved membrane design, *AIChE J.* **53**, 2007. doi:10.1002/aic.11197.

25) S. Liang, Performance Modeling and Analysis of a Hollow Fiber Membrane System, *J. Membr.Sci. Technol*. **06**, 2016. doi:10.4172/2155-9589.1000144.

26) S. Boributh, W. Rongwong, S. Assabumrungrat, N. Laosiripojana, R. Jiraratananon, Mathematical modeling and cascade design of hollow fiber membrane contactor for CO2 absorption by monoethanolamine, *J. Membr. Sci*. **401-402**, 2012. doi:10.1016/j.memsci.2012.01.048.

27) L. Theodore, R. R. Dupont, K. Ganesan Characteristics of Mass Transfer Operations, Unit Operations in Environmental Engineering. 2017, 471–481. doi:10.1002/9781119283706.ch47.

28) E. Romeo, C. Royo, A. Monzón, Improved explicit equations for estimation of the friction factor in rough and smooth pipes, *Chem. Eng. J.* **86**, 2002. doi:10.1016/s1385-8947(01)00254-6.

29) J.E. Helt, M.A. Larson, Effects of temperature on the crystallization of potassium nitrate by direct measurement of supersaturation, *AIChE J*. **23**, 1977. doi:10.1002/aic.690230608.

30) C. M. Narayanan, B.C. Bhattacharya, Unit operations and unit processes: including computer programs, CBS Publishers & Distributors, New Delhi, 2007.

31) P. Das, S. Dutta, K. Singh, S. Maity, Energy saving integrated membrane crystallization: A sustainable technology solution, *Sep. Purif. Technol*. **228**, 2019. doi:10.1016/j.seppur.2019.115722.

32) Determination of glucose using titration, Determination of Glucose Using Titration - TecHKnow Wiki. (n.d.). http://www.techknow.org.uk/wiki/index.php?title=Determination_of_glucose_using_titration (accessed April 18, 2022).

33) R.J. Kerekess, C.J. Schell, Characterization of fibre flocculation regimes by a crowding factor. *J. Pulp Pap. Sci.* **18** , 1992

34) D. Chang, J. Min, S. Oh, K. Moon, Effect of pressure drop on performance of hollow-fiber membrane module for gas permeation, Korean J. Chem. Eng. 15 1998. doi:10.1007/bf02697129.

35) D. Li, R. Wang, T.-S. Chung, Fabrication of lab-scale hollow fiber membrane modules with high packing density, *Sep. Purif. Technol*. **40**, 2004. doi:10.1016/j.seppur.2003.12.019.

36) I. Borsi, O. Lorain, A space-averaged model for hollow fibre membranes filters, *Comput. Chem. Eng*. **39** (2012) 65–74. doi:10.1016/j.compchemeng.2011.12.017.

37) C.-H. Shin, J.-M.Seo, J.-S.Bae, Modification of a hollow fiber membrane and its three-dimensional analysis of surface pores and internal structure for a water reclamation system, *J. Ind. Eng. Chem*. **15**, 2009. doi:10.1016/j.jiec.2009.05.001.

38) P. Luis, Membrane contactors, Fundamental Modelling of Membrane Systems. 2018. doi:10.1016/b978-0-12-813483-2.00005-8.

39) Q. Xia, H. Guo, Y. Ye, S. Yu, L. Li, Q. Li, et al., Study on the fouling mechanism and cleaning method in the treatment of polymer flooding produced water with ion exchange membranes, *RSC Adv.* **8** , 2018. doi:10.1039/c8ra05575k.

40) E. Demirhan, D.K. Apar, B. Özbek, A modelling study on hydrolysis of whey lactose and stability of β-galactosidase, Korean J Chem Eng. **27**, 2010. doi:10.1007/s11814-010-0062-5.

41) G.D. Profio, E. Curcio, A. Cassetta, D. Lamba, E. Drioli, Membrane crystallization of lysozyme: kinetic aspects, *J. Cryst. Growth*. **257**, 2003. doi:10.1016/s0022-0248(03)01462-3.

42) A.B.N. Brito, M. Giulietti, Study of lactose crystallization in water-acetone solutions, *Cryst. Res. Technol*. **42**, 2007. doi:10.1002/crat.200610867.

43) U. Domańska, A. Marciniak, Solubility of Ionic Liquid [emim][PF6] in Alcohols, *The J. Phys. Chem. B*. **108**, 2004. doi:10.1021/jp030582h.

44) J. Warfsmann, B. Tokay, N.R. Champness, Synthesis of hydrophobic MIL-53(Al) nanoparticles in low molecular weight alcohols: systematic investigation of solvent effects, *CrystEngComm*. **20**, 2018. doi:10.1039/c8ce00913a.

45) J. Cho, G. Amy, J. Pellegrino, Membrane filtration of natural organic matter: initial comparison of rejection and flux decline characteristics with ultrafiltration and nanofiltration membranes, *Water Res.* **33**, 1999. doi:10.1016/s0043-1354(98)00498-9.

46) R. Atra, G. Vatai, E. Bekassy-Molnar, A. Balint, Investigation of ultra- and nanofiltration for utilization of whey protein and lactose, *J. Food Eng*. **67**, 2005. doi:10.1016/j.jfoodeng.2004.04.035.

Declaration :

The authors declare there is no conflict of interest in the manuscript.

The data will be available on reasonable request.